Published as: *Nature*. 2006 April 27; 440(7088): 1213–1216.

A voltage-gated proton-selective channel lacking the pore domain

I. Scott Ramsey[1], **Magdalene M. Moran**[1,†], **Jayhong A. Chong**[1,†], and **David E. Clapham**[1]

[1]Howard Hughes Medical Institute, Department of Cardiology, Children's Hospital, Department of Neurobiology, Harvard Medical School, Enders 1309, 320 Longwood Avenue, Boston, Massachusetts 02115, USA

Abstract

Voltage changes across the cell membrane control the gating of many cation-selective ion channels. Conserved from bacteria to humans[1], the voltage-gated-ligand superfamily of ion channels are encoded as polypeptide chains of six transmembrane-spanning segments (S1–S6). S1–S4 functions as a self-contained voltage-sensing domain (VSD), in essence a positively charged lever that moves in response to voltage changes. The VSD 'ligand' transmits force via a linker to the S5–S6 pore domain 'receptor'[2], thereby opening or closing the channel. The ascidian VSD protein Ci-VSP gates a phosphatase activity rather than a channel pore, indicating that VSDs function independently of ion channels[3]. Here we describe a mammalian VSD protein (H_V1) that lacks a discernible pore domain but is sufficient for expression of a voltage-sensitive proton-selective ion channel activity. H_v1 currents are activated at depolarizing voltages, sensitive to the transmembrane pH gradient, H^+-selective, and Zn^{2+}-sensitive. Mutagenesis of H_v1 identified three arginine residues in S4 that regulate channel gating and two histidine residues that are required for extracellular inhibition of H_v1 by Zn^{2+}. H_v1 is expressed in immune tissues and manifests the characteristic properties of native proton conductances (G_{vH^+}). In phagocytic leukocytes[4], G_{vH^+} are required to support the oxidative burst that underlies microbial killing by the innate immune system[4,5]. The data presented here identify H_v1 as a long-sought voltage-gated H^+ channel and establish H_v1 as the founding member of a family of mammalian VSD proteins.

H_v1 was identified as a novel conserved human gene using bioinformatic searches based on known cation channels. The *H_v1* gene is located on chromosome 12 at q24.11 and is encoded by seven exons, the first of which is predicted to be non-coding. H_v1 messenger RNA is encoded by multiple independent human expressed sequence tags that contain in-frame stop codons preceding the initiator ATG and 3′ poly-A^+ tails. The predicted H_v1 protein is 273 amino acids in length (31.7 kDa, pI = 6.62) and forms four transmembrane segments (S1–S4), according to hydropathy analyses (Supplementary Fig. S1a, b). The

---

Correspondence and requests for materials should be addressed to: D.E.C. (dclapham@enders.tch.harvard.edu).
†Present address: Hydra Biosciences, 790 Memorial Drive, Cambridge, Massachusetts 02139, USA.

Supplementary Information is linked to the online version of the paper at www.nature.com/nature.

The authors declare no competing financial interests.

overall transmembrane (TM) structure and placement of charged residues in hydrophobic domains is conserved among the vertebrate H_v1 orthologues (Supplementary Fig. S1a) and similar to both Ci-VSP (ref. 3) and the VSD of $K_v1.2$ (ref. 2). The amino-terminal ~100 amino acids in H_v1 are homologous to protein and lipid phosphatases, but unlike the catalytically active Ci-VSP, core active site residues required for phosphatase activity[6] are not conserved in H_v1.

Both the distribution of expressed sequence tags (UniGene, see http://www.ncbi.nlm.nih.gov/UniGene/ESTProfileViewer.cgi?uglist=Hs.334637) and high-throughput expression studies (GNF Sym-Atlas, see http://symatlas.gnf.org/SymAtlas/; search on MGC15619 protein) indicate that *H_v1* mRNA is enriched in immune tissues such as lymph node, B-lymphocytes, monocytes and spleen. We found marked lymph node expression of *H_v1* mRNA on a human RNA dot blot (Supplementary Fig. S1d, spot F7). H_v1 protein expression was detected with an affinity-purified rabbit polyclonal anti-peptide antibody that recognizes H_v1, green flurorescent protein (GFP)-H_v1 and H_v1-haemagglutinin (HA) at their appropriate molecular weights in western blots of transfected HEK cells, but not mock-transfected controls (Supplementary Fig. S2b). The antibody recognized H_v1 in human immune tissues including lymph node (Supplementary Fig. S2a), and the human leukocyte cell lines HL-60 and Jurkat (Supplementary Fig. S2b, c).

In preliminary experiments, we observed large (>1 nA at +100 mV) voltage-dependent, outwardly rectifying whole-cell currents in transfected HEK cells bathed in standard Ringer's, low-Cl^- (where all but 8 mM Cl^- was substituted with NO_3^-, SCN^- or Br^-), or $NMDG^+$ (N-methyl-D-glucamine) · Cl (Na^+, K^+, Ca^{2+} and Mg^{2+} -free) solutions, suggesting that H_v1 currents were primarily permeable to H^+. To study H^+ currents under better pH control, we used solutions with high H^+ buffering capacity (100 mM buffer used near its pK_a: MES, pH 5.5; Bis-Tris, pH 6.5; HEPES, pH 7.5) similar to those used previously to study native G_{vH^+} (refs 7, 8). In response to depolarizing voltage steps, cells transfected with H_v1 generated time-, voltage-, and pH-dependent currents with relatively slow activation kinetics and a rapidly decaying inward tail current (Fig. 1a–c). The kinetics of H_v1 activation (τ_{act} = 715 ± 124 ms) and deactivation (τ_{deact} = 65.0 ± 12.1 ms) were estimated from single exponential fits to the currents at +80 mV or −80 mV, respectively. Both τ_{act} and τ_{deact} are strongly voltage-dependent (Fig. 1e) and τ_{act} was noticeably variable between experiments, perhaps owing to small fluctuations in room temperature and the highly temperature-sensitive gating of H_v1 (Supplementary Fig. S3c, d).

In the absence of a H^+ gradient (the ratio of internal to external H^+ concentration $\rho H^+_{i/o}=1.0$), the voltage threshold (V_{thr}) for activation of outward currents (I_{step}) was 11 mV (Fig. 1d). An outwardly directed H^+ gradient, equivalent to net intracellular acidification ($\rho H^+_{i/o}=10$), caused V_{thr} to shift 40 mV negative (Fig. 1d). The reversal potential (E_{rev}) of open H_v1 channels determined from I_{tail} (Fig. 1e) was ~0 mV under symmetrical recording conditions ($\rho H^+_{i/o}=1$) and shifted >50 mV negative or positive in inward ($\rho H^+_{i/o}=0.1$) or outward ($\rho H^+_{i/o}=10$) H^+ gradients, respectively (Fig. 1f). A plot of E_{rev} versus $[H^+]$ was well fitted to a line with slope = 54.7 mV/log$[H^+]$ (data not shown), indicating that the H_v1

current was highly selective for H^+. A plot of V_{thr} versus the calculated Nernst potential for H^+ was well fitted by the line $V_{thr} = 0.82\ E_{rev} + 13.8$ mV (Fig. 1g).

Although the outwardly rectifying I_{step}–V relation was linear at voltages ~10–70 mV positive to E_{rev} (Fig. 1d, Fig. 2a, c), we were surprised to find that the H_v1 I_{step}–V deviated from linearity and appeared to saturate at voltages ~100 mV positive to E_{rev} (Fig. 2a, c). We infer that the apparent nonlinearity in I_{step} results from depletion of H_i^+ caused by rapid channel-mediated H^+ efflux that is not adequately compensated by delivery of H_i^+ from the buffer during the voltage step. Slow H_v1 kinetics near V_{thr} further hinder our ability to measure accurately the channels' voltage dependence because extraordinarily long voltage pulses are required to reach true steady state. Erosion of the H^+ gradient during I_{step} and under-estimation of I_{step} are both expected to flatten the I_{tail}–V relation. We were nonetheless able to fit H_v1 I_{tail}–V relations ($\rho H^+_{i/o}=10$) to a Boltzmann function in order to approximate the voltage-dependence of the H_v1 open channel probability (P_o, Fig. 2c). In an outward H^+ gradient, H_v1 channels appear to be half open at ~60 mV and to move the equivalent of about one electronic charge across the membrane during channel opening ($z\delta$ = 0.9). The midpoint of the I_{step}–V relation shifted >40 mV when the H^+ gradient was altered, consistent with the observed shift in V_{thr} (Fig. 1).

In an initial attempt to determine whether voltage-dependent gating in H_v1 involved basic residues in S4, as it does in other voltage-gated channels, we individually replaced each of three arginine residues with alanine. Representative traces from cells expressing H_v1 or the point mutant R205A are shown in Fig. 2a, b. Relative to H_v1, two arginine mutants (R205A, R208A) exhibited dramatically faster activation and deactivation kinetics, whereas R211A exhibited only faster deactivation kinetics (Supplementary Fig. S3e–g). R205A exhibited a positive shift in the half-maximal voltage for channel activation ($V_{0.5}$) and a statistically significant decrease in the slope factor ($z\delta$) derived from Boltzmann fits to I_{tail}–V (Fig. 2c).

Like G_{vH^+}, H_V1 current was rapidly and reversibly blocked by bath superfusion of $ZnCl_2$ in the absence of EGTA (Fig. 3a, e). We therefore mutated putatively extracellular residues that might co-ordinate metal ions to inhibit H_v1 currents. Zn^{2+} potently inhibited I_{Hv1} (half-maximal inhibitory concentration, $IC_{50} \approx 2$ μM) and slowed τ_{act} (Fig. 3a–c, data not shown). Apparent Zn^{2+} potency decreased 10- or 30-fold when we mutated H193 or H140 to alanine, respectively. Mutation of both residues (H140A/H193A) practically abolished Zn^{2+} sensitivity (Fig. 3d). All three histidine mutants exhibited the expected H^+-selectivity and $\rho H^+_{i/o}$-dependent shift in V_{thr} that are characteristic of H_v1 (data not shown).

The surprising finding of this study is that expression of a voltage-sensor domain, without its normally associated pore domain, is sufficient to reconstitute voltage-dependent proton channel activity. G_{vH^+} have been recorded in a wide variety of cells from molluscs[9] to mammals (reviewed in ref. 4). In mammalian phagocytes, G_{vH^+} provides necessary charge compensation for the gp91^{phox} electron current that underlies Zn^{2+}-sensitive superoxide anion production[4,5,10,11]. Loss of functional gp91^{phox} in humans causes X-linked chronic granulomatous disease, which is characterized by decreases in microbial killing by phagocytes[12,13].

The properties of expressed H_v1 are consistent with those of G_{vH^+} (refs 4, 14, 15). H_v1 is H^+-selective, exhibits a −40 mV shift in V_{thr} when pH_i is decreased one unit, is blocked by micromolar Zn^{2+}, and is highly temperature sensitive. H_v1 kinetics fall within the range reported for G_{vH^+} in a variety of mammalian cells[4]. Kinetic heterogeneity among native G_{vH^+} could reflect the existence of unidentified H_v1 homologues, temperature differences during recording, post-translational modification of H_v1, or second-messenger modulation of H^+ channels. The small endogenous G_{vH^+} reported in HEK[16] and CHO[17] (but not COS-7[18]) cells appeared neither to facilitate nor interfere with expression of H_v1 current in this study. Slow activation kinetics and large H^+ currents in H_v1-transfected cells will tend to exacerbate difficulties in measuring steady-state channel behaviour and in maintaining the imposed H^+ gradient during strongly depolarizing voltage pulses, and could explain why the voltage dependence of expressed H_v1 channels appears shallow relative to native currents[4].

An accepted model for voltage-gated channels is one in which positively charged residues in S4 function as the primary voltage sensors[19,20]. Charge-neutralizing mutagenesis of S4 arginine residues (R205A, R208A, R211A) demonstrates that these basic residues are intimately involved in H_v1 gating and may directly sense transmembrane voltage. Voltage-dependent gating in H_v1 is distinguished from other cation channels by its sensitivity to a H^+ gradient, indicating that further studies are required to clarify whether the mechanism of voltage sensing in H_v1 is similar to that in other voltage-gated channels. Starace and Bezanilla[21] replaced an S4 arginine in *Shaker* with histidine (R362H) to create aH^+-permeable channel at negative membrane potentials. In H_v1, neutralizing S4 arginines or histidines in the extracellular linkers did not prevent the H^+ conductance, indicating that H^+ permeation does not require proton acceptors at these positions. Mutagenesis of putative H^+ acceptors may be of limited use in defining the conduction pathway given that H^+ conductance could be indirectly attenuated owing to allosteric effects. The mechanism of proton permeation may involve a voltage-dependent movement of S4 to align residues that create a ‘proton wire’, as in gramicidin[22], or exposure of an H^+ acceptor that bridges two water-filled crevices[21]. The latter model unites both pore and wire features in that the proton acceptor can also be thought of as the binding site for H^+ within a pore that confers H^+ selectivity.

Polyvalent cations, particularly Zn^{2+}, are the only known blockers of native G_{vH^+} (refs 4, 15). Zn^{2+} block of native proton current was predicted to involve two extracellularly accessible amino acids; apparent Zn^{2+} potency is modulated by both $[H^+]_o$ and membrane voltage[15]. Strikingly, we identified two histidine residues that appear to function coordinately to confer Zn^{2+} inhibition to H_v1. In addition, Zn^{2+} slows τ_{act}, mirroring its effect on G_{vH^+} (ref. 15) and further supporting the conclusion that H_v1 activity underlies native G_{vH^+}.

Expression of H_v1 alone is sufficient to reconstitute most properties of G_{vH^+}, making it unlikely that G_{vH^+} is mediated by $gp91^{phox}$ (refs 23, 24). Future studies are required to ascertain whether H_v1 physically associates with or is regulated by components of the NADPH oxidase complex, protein kinase C, or arachidonic acid[25–27], whether H_v1 channel activity is sufficient to control O_2^- secretion and reactive oxygen species production[28,29], and what factors account for differences between ‘phagocyte’ and ‘epithelial’ type G_{vH^+} (ref. 4).

Finally, future structural and biophysical studies should help to elucidate the proton permeation pathway within this voltage sensor domain protein.

Note added in proof: Okamura and colleagues also report that the mouse *Hv1* gene encodes a proton channel, which they call VSOP (voltage-sensor only protein)[30].

METHODS

H_v1 complementary DNA was amplified by polymerase chain reaction (PCR) from an expressed sequence tag clone (IMAGE 6424182) and subcloned into pQBI25-fC3 (QBiogene) to create *GFP–H_v1*, pcDNA3.1(−) for expression of non-tagged *H_v1*, or pBSIISK – (Stratagene) for *in vitro* mRNA transcription. Site-directed mutagenesis was used to create point mutations in *GFP–H_v1: H140A*, *H193A*, *R205A*, *R208A*, *R211A*, and the *H140A/H193A* double mutant; *H_v1-HA* was used for biochemical studies. A ~300 nucleotide antisense RNA probe labelled with α-^{33}P-UTP was synthesized by *in vitro* transcription (Ambion) and hybridized (68 °C) to a human multiple tissue mRNA panel (MTE3, Clontech). Incorporated radioactivity was detected by a phosphorimager (Molecular Dynamics).

Currents reported here were recorded 18–36 h after transfection of *GFP–H_v1* cDNA in the HEK-293 cell clone HM1. Recording solutions were similar to those described previously[18] and contained 100 mM pH buffer (MES, Bis-Tris or HEPES) near its pK_a (5.5, 6.5 or 7.5, respectively) in tetramethylammonium methanesulphonate or NaCl adjusted to ~300 mOsm. H^+ gradients ($\rho H^+_{i/o} = [H_+]_{intracellular}/[H^+]_{extracellular}$) were imposed by gravity-fed bath superfusion of differentially buffered solutions. Currents were recorded with an Axopatch 200 A (Axon Instruments; 1 kHz filter) and digitized at 2 kHz (10 kHz for Arg mutants) using Clampex9 (Axon Instruments). Data were analysed using Clampfit9 (Axon Instruments) and Origin 6 (Microcal). Recordings were performed at 22–24 °C unless otherwise stated. Data shown and stated in text and legends represent mean ± s.e.m. for the indicated number of experiments.

Affinity-purified 4234 polyclonal rabbit antibodies (Chemicon) were raised against the keyhole limpet haemocyanin (KLH)-conjugated H_v1 peptide CSEKEQEIERLNKL. Transfected cells were lysed in 1% Triton X-100 and crude membranes were subjected to SDS–polyacrylamide gel electrophoresis (PAGE) (NuPage, Invitrogen). Following transfer to nitrocellulose, blots were probed with the indicated concentration of 4234 followed by an anti-rabbit HRP-conjugated secondary antibody (Zymed). Immunoreactivity was detected by enhanced chemiluminescence (Pierce). A human immune tissue western blot (1525, ProSci) was probed with 4234 as described.

Supplementary Material

Refer to Web version on PubMed Central for supplementary material.

Acknowledgments

We thank T. DeCoursey, C. Miller, R. MacKinnon and P. Bezanilla for comments on the manuscript, and K.-H. Lee for technical assistance. This work was supported by the Sandler Program for Asthma Research and the Howard Hughes Medical Institute.

References

1. Yu FH, Catterall WA. The VGL-chanome: a protein superfamily specialized for electrical signaling and ionic homeostasis. Sci STKE. 2004; 2004:re15. [PubMed: 15467096]
2. Long SB, Campbell EB, Mackinnon R. Crystal structure of a mammalian voltage-dependent Shaker family K^+ channel. Science. 2005; 309:897–903. [PubMed: 16002581]
3. Murata Y, Iwasaki H, Sasaki M, Inaba K, Okamura Y. Phosphoinositide phosphatase activity coupled to an intrinsic voltage sensor. Nature. 2005; 435:1239–1243. [PubMed: 15902207]
4. DeCoursey TE. Voltage-gated proton channels and other proton transfer pathways. Physiol Rev. 2003; 83:475–579. [PubMed: 12663866]
5. DeCoursey TE, Morgan D, Cherny VV. The voltage dependence of NADPH oxidase reveals why phagocytes need proton channels. Nature. 2003; 422:531–534. [PubMed: 12673252]
6. Goldberg J, et al. Three-dimensional structure of the catalytic subunit of protein serine/threonine phosphatase-1. Nature. 1995; 376:745–753. [PubMed: 7651533]
7. Schilling T, Gratopp A, DeCoursey TE, Eder C. Voltage-activated proton currents in human lymphocytes. J Physiol (Lond). 2002; 545:93–105. [PubMed: 12433952]
8. DeCoursey TE, Cherny VV, DeCoursey AG, Xu W, Thomas LL. Interactions between NADPH oxidase-related proton and electron currents in human eosinophils. J Physiol (Lond). 2001; 535:767–781. [PubMed: 11559774]
9. Thomas RC, Meech RW. Hydrogen ion currents and intracellular pH in depolarized voltage-clamped snail neurones. Nature. 1982; 299:826–828. [PubMed: 7133121]
10. Henderson LM, Chappell JB, Jones OT. Superoxide generation by the electrogenic NADPH oxidase of human neutrophils is limited by the movement of a compensating charge. Biochem J. 1988; 255:285–290. [PubMed: 2848506]
11. Rada BK, Geiszt M, Kaldi K, Timar C, Ligeti E. Dual role of phagocytic NADPH oxidase in bacterial killing. Blood. 2004; 104:2947–2953. [PubMed: 15251984]
12. Babior BM. NADPH oxidase. Curr Opin Immunol. 2004; 16:42–47. [PubMed: 14734109]
13. Smith RM, Curnutte JT. Molecular basis of chronic granulomatous disease. Blood. 1991; 77:673–686. [PubMed: 1993212]
14. DeCoursey TE, Cherny VV. Temperature dependence of voltage-gated H^+ currents in human neutrophils, rat alveolar epithelial cells, and mammalian phagocytes. J Gen Physiol. 1998; 112:503–522. [PubMed: 9758867]
15. Cherny VV, DeCoursey TE. pH-dependent inhibition of voltage-gated H^+ currents in rat alveolar epithelial cells by Zn^{2+} and other divalent cations. J Gen Physiol. 1999; 114:819–838. [PubMed: 10578017]
16. Eder C, DeCoursey TE. Voltage-gated proton channels in microglia. Prog Neurobiol. 2001; 64:277–305. [PubMed: 11240310]
17. Cherny VV, Henderson LM, DeCoursey TE. Proton and chloride currents in Chinese hamster ovary cells. Membr Cell Biol. 1997; 11:337–347. [PubMed: 9460053]
18. Morgan D, Cherny VV, Price MO, Dinauer MC, DeCoursey TE. Absence of proton channels in COS-7 cells expressing functional NADPH oxidase components. J Gen Physiol. 2002; 119:571–580. [PubMed: 12034764]
19. Bezanilla F. The voltage sensor in voltage-dependent ion channels. Physiol Rev. 2000; 80:555–592. [PubMed: 10747201]
20. Tombola F, Pathak MM, Isacoff EY. How far will you go to sense voltage? Neuron. 2005; 48:719–725. [PubMed: 16337910]

21. Starace DM, Bezanilla F. A proton pore in a potassium channel voltage sensor reveals a focused electric field. Nature. 2004; 427:548–553. [PubMed: 14765197]
22. Pomes R, Roux B. Molecular mechanism of H^+ conduction in the single-file water chain of the gramicidin channel. Biophys J. 2002; 82:2304–2316. [PubMed: 11964221]
23. DeCoursey TE, Morgan D, Cherny VV. The gp91phox component of NADPH oxidase is not a voltage-gated proton channel. J Gen Physiol. 2002; 120:773–779. [PubMed: 12451047]
24. Henderson LM, Meech RW. Evidence that the product of the human X-linked CGD gene, gp91-phox, is a voltage-gated H^+ pathway. J Gen Physiol. 1999; 114:771–786. [PubMed: 10578014]
25. Bokoch GM. Regulation of innate immunity by Rho GTPases. Trends Cell Biol. 2005; 15:163–171. [PubMed: 15752980]
26. DeCoursey TE, Cherny VV, Morgan D, Katz BZ, Dinauer MC. The gp91phox component of NADPH oxidase is not the voltage-gated proton channel in phagocytes, but it helps. J Biol Chem. 2001; 276:36063–36066. [PubMed: 11477065]
27. Price MO, et al. Creation of a genetic system for analysis of the phagocyte respiratory burst: high-level reconstitution of the NADPH oxidase in a nonhematopoietic system. Blood. 2002; 99:2653–2661. [PubMed: 11929750]
28. Bokoch GM, Knaus UG. NADPH oxidases: not just for leukocytes anymore! Trends Biochem Sci. 2003; 28:502–508. [PubMed: 13678962]
29. Qu AY, Nanda A, Curnutte JT, Grinstein S. Development of a H^+-selective conductance during granulocytic differentiation of HL-60 cells. Am J Physiol. 1994; 266:C1263–C1270. [PubMed: 8203491]
30. Sasaki M, Takagi M, Okamura Y. A novel protein with a voltage sensor domain is a voltage-gated proton channel. Science. (in the press).

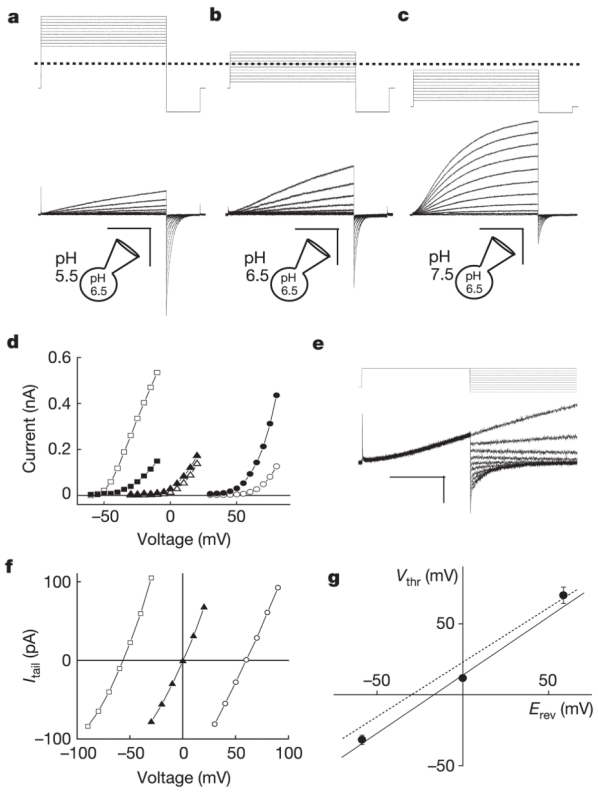

Figure 1. Biophysical properties of expressed H_v1 currents

Depolarizing voltage steps (5 mV increments) were applied to an *H_v1*-transfected HM1 cell (**a**–**c**) to elicit outward H^+ currents and deactivating inward tail currents (−80 mV). $TMA5.5_o$, $TMA6.5_o$ or $TMA7.5_o$ ($TMA6.5_i$ for all) were used to impose pH gradients indicated in the diagrams. **a**, $\rho H^+_{i/o}=0.1$, V_h = −40 mV (V_{step} = +30 mV to +80 mV, scale bar 0.2 nA, 1 s; **b**, $\rho H^+_{i/o}=1$, V_h = −40 mV (V_{step} = −30 mV to +20 mV), scale bar 0.1 nA, 1 s; **c**, $\rho H^+_{i/o}=10$, V_h = −70 mV (V_{step} = −60 mV to −10 mV), scale bar 0.2 nA, 1 s. **d**, H_v1 currents at the end of the depolarizing step (I_{step}, open symbols) and the absolute value of I_{tail} (−80 mV, filled symbols) are plotted as a function of the step voltage. Data shown are from the cell shown in **a**–**c**. Circles, $\rho H^+_{i/o}=0.1$ (V_{thr} = 70 ± 5.8 mV, n = 3); triangles, $\rho H^+_{i/o}=1.0$ (V_{thr} = 11.7 ± 2.1 mV, n = 6); squares, $\rho H^+_{i/o}=10$ (V_{thr} = −31.7 ± 3.3 mV, n = 3). **e**, Representative currents for E_{rev} measurement (V_h = −40 mV, V_{step} = +40 mV, V_{tail} = −100 mV to +40 mV). Small I_{step} (<200 pA) was chosen to minimize H^+_i depletion (note constant outward current level). **f**, Monoexponential fits of I_{tail} were extrapolated to t = 0 and E_{rev} was estimated from the zero-current intercept of linear fits to the data. Open circles, $TMA6.5_i$, $TMA5.5_o$ ($\rho H^+_{i/o}=0.1$); filled triangles, $TMA6.5_i$, $TMA6.5_o$ ($\rho H^+_{i/o}=1$); open squares, $TMA6.5_i$, $TMA7.5_o$ ($\rho H^+_{i/o}=10$). Average E_{rev} values: E_{rev} = 53.3 ± 1.4 mV, $\rho H^+_{i/o}=0.1$, n = 10; E_{rev} = 0.9 ± 0.7 mV, $\rho H^+_{i/o}=1.0$, n = 14; E_{rev} = −56.5 ± 2.6 mV, $\rho H^+_{i/o}=10$, n = 5. Data represent mean ± s.e.m. from n experiments. **g**, V_{thr} is plotted against

the Nernst potential for H^+ at 24 °C. The data are fitted to $V_{thr} = 0.82\ E_{rev} + 13.8$ mV (solid line). Data represent mean ± s.e.m. from $n = 3–7$ experiments. The V_{thr} versus E_{rev} relationship for native G_{vH^+} ($V_{thr} = 0.79\ E_{rev} + 23$ mV[4], dotted line) is shown for comparison.

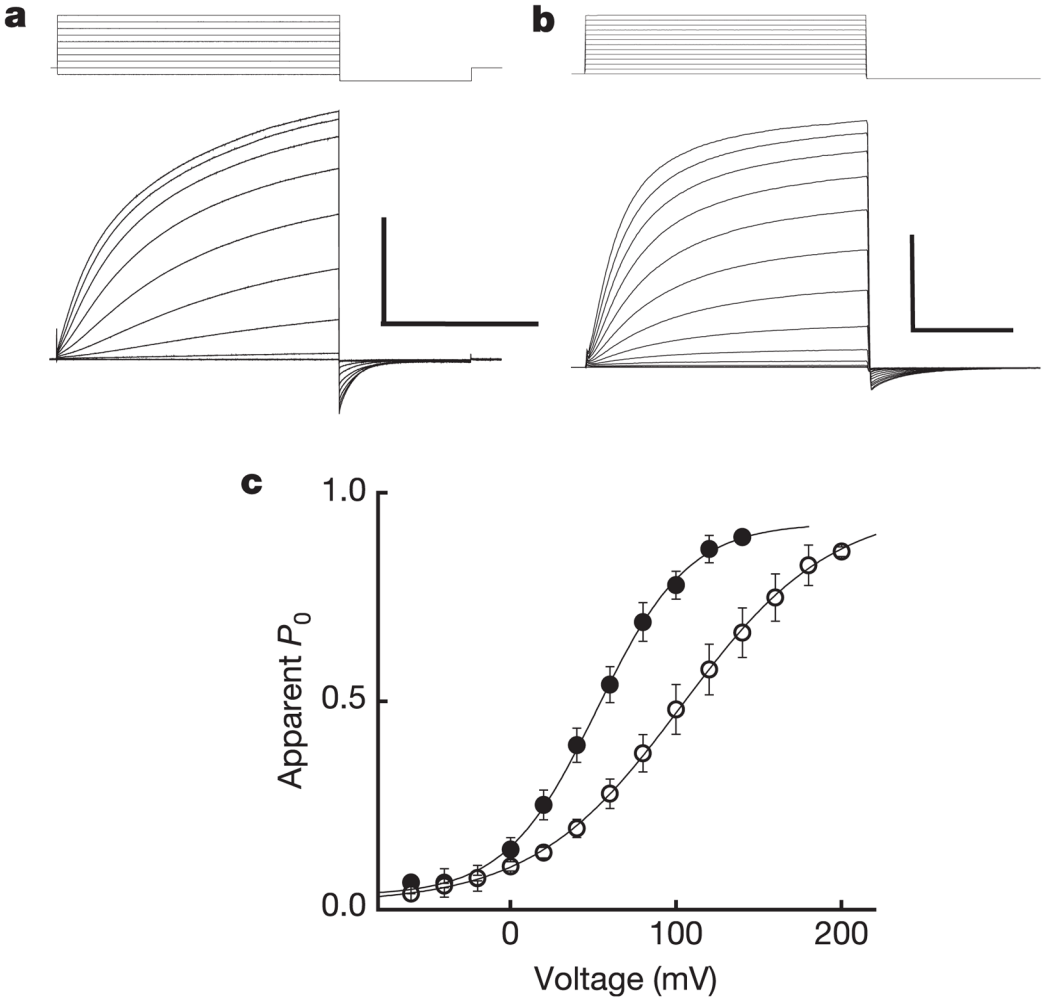

Figure 2. H_v1 voltage-dependent gating

a, H_v1 currents (−60 mV to +120 mV, V_h = −40 mV, $\rho H^+_{i/o}=10$, $Na6.5_i$, $Na7.5_o$) in a representative cell. Scale bar 2 nA, 400 ms. Under symmetrical conditions (TMA6.5, $\rho H^+_{i/o}=1$), τ_{act} = 715 ± 124 ms (+80 mV), n = 9 and τ_{deact} = 65.0 ± 12.1 ms (−80 mV), n = 7. **b**, R205A (−60 mV to +180 mV, V_h = −60 mV, $\rho H^+_{i/o}=10$, $Na6.5_i$, $Na7.5_o$). Scale bar 2 nA, 10 ms. Note the 40-fold difference in timescale compared to **a. c**, The I_{tail}–V relation (−80 mV, $\rho H^+_{i/o}=10$, $Na6.5_i$, $Na7.5_o$) was normalized to the maximum current obtained from a Boltzmann fit to the data for each cell expressing H_v1 (filled circles) or R205A (open circles) to estimate $P_o - V$. Data were fitted to a Boltzmann function (solid lines) and normalized to the extrapolated maximum current. Points represent mean ± s.e.m. of normalized data. A comparison of curve fits from individual experiments (H_v1, $V_{0.5}$ = 58.0 ± 5.6 mV, $z\delta$ = 0.90 ± 0.04, n = 6; R205A, $V_{0.5}$ = 99.5 ± 18.3 mV, $z\delta$ = 0.57* ± 0.03, n = 3; *P = 0.03 by Student's non-paired t-test) indicates that significantly less effective charge is moved in R205A than in H_v1 during channel gating. Data represent mean ± s.e.m. from n experiments.

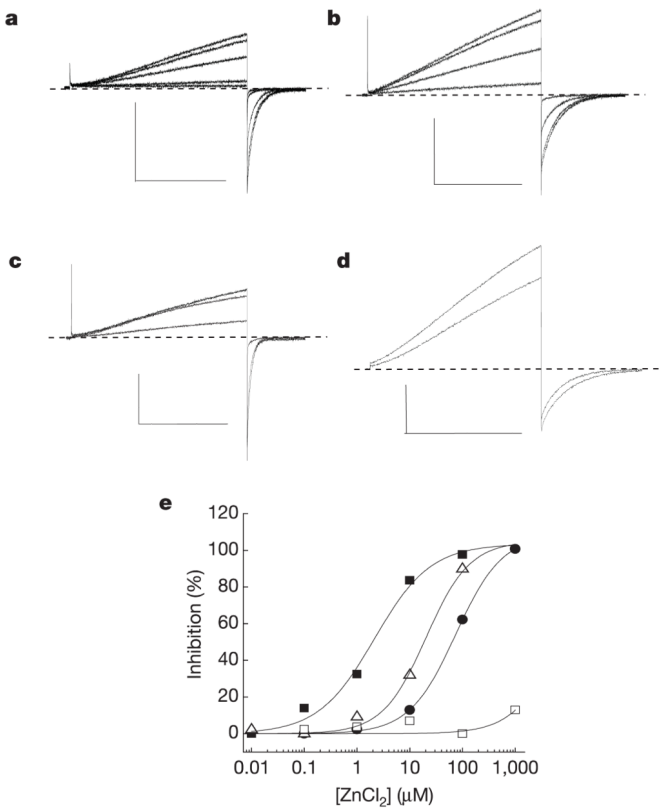

Figure 3. Mutations in H_v1 reveal residues required for Zn^{2+} inhibition

Inhibition of I_{step} (+25 mV to +50 mV) in cells superfused with EGTA-free TMA6.5 or Na6.5 ($\rho H^+_{i/o}=1$) was typically faster than the sampling interval (10 s) and washout was always complete. Average IC_{50} = 2.2 ± 0.6 μM, n_H = 1.0 ± 0.2, n = 4; $\rho H^+_{i/o}=1$, + 40 mV, TMA6.5. Data represent mean ± s.e.m. from n experiments. The applied voltages and $[Zn^{2+}]$ for the records shown (Na6.5, $\rho H^+_{i/o}=1$) were: **a**, H_v1, V_{step} = +40/V_{tail} = −80 mV, $[Zn^{2+}]$ = 0, 0.1, 1, 10, 100 μM; **b**, H140A, +40/−60 mV, $[Zn^{2+}]$ = 0, 1, 10, 100 μM; **c**, H193A, +30/−80 mV, $[Zn^{2+}]$ = 0, 10, 100 μM; **d**, H140A/H193A, +50/−20 mV, $[Zn^{2+}]$ = 0, 1 mM. Scale bars: 100 pA, 1 s. **e**, Representative Zn^{2+} concentration-response curves for H_v1 (filled squares, IC_{50} = 1.9 μM, n_H = 0.9), H193A (open triangles, IC_{50} = 17.9 μM, n_H = 1.2), H140A (filled circles, IC_{50} = 74.3 μM, n_H = 1.0), and H140A/H193A (open squares, maximum inhibition = 11.1 ± 3.4%, n = 3).